

## Long-Wavelength Optical Lattice Vibrations in $\text{Ba}_y\text{Sr}_{1-y}\text{F}_2$ and $\text{Sr}_y\text{Ca}_{1-y}\text{F}_2$

H. W. VERLEUR AND A. S. BARKER, JR.

*Bell Telephone Laboratories, Murray Hill, New Jersey*

(Received 11 July 1967)

The far-infrared reflectivity spectra of  $\text{Sr}_y\text{Ca}_{1-y}\text{F}_2$  and  $\text{Sr}_y\text{Ba}_{1-y}\text{F}_2$  have been measured both at room temperature and at 100°K over the spectral range from 10 to 100  $\mu$ . Chang *et al.* have observed a single Raman mode in these crystals and suggested that a virtual-ion model is applicable. This is to be distinguished from such systems as  $\text{GaAs}_y\text{P}_{1-y}$  and  $\text{CdSe}_y\text{S}_{1-y}$  where the appearance of two reststrahlen bands leads to a more complicated model. Even though the reflectivity spectra of these mixed fluorides show essentially a single reststrahlen band, these bands have some fine structure. The infrared reststrahlen band shifts smoothly but in a nonlinear manner with  $y$ . The model used previously for  $\text{GaAs}_y\text{P}_{1-y}$  is adapted to the present case and is shown to predict both the Raman and infrared spectra including the fine structure. The model shows that the virtual-ion approximation is valid for the main Raman mode but not for the infrared modes. Contrary to the case of  $\text{GaAs}_y\text{P}_{1-y}$ , no significant clustering of like cations around anions is detected.

### I. INTRODUCTION

RECENTLY Chang, Lacina, and Pershan<sup>1</sup> studied Raman scattering from the mixed crystals  $\text{Ba}_y\text{Sr}_{1-y}\text{F}_2$  and  $\text{Sr}_y\text{Ca}_{1-y}\text{F}_2$ . They found that just as in the parent crystals, only a single Raman-active mode is observed in the mixed crystals. The frequency of this mode varies linearly with concentration  $y$ . Somewhat similar results were obtained for the infrared-active mode in  $\text{Co}_y\text{Ni}_{1-y}\text{O}$  by Gielisse *et al.*<sup>2</sup>

We may contrast mixed-crystal systems of this kind, in which the lattice vibrational properties appear to be an average of those of the parent crystals, with other mixed-crystal systems in which two distinct sets of optical lattice modes are observed.<sup>3</sup> Examples of mixed crystals showing two-band behavior are  $\text{GaAs}_y\text{P}_{1-y}$ ,<sup>4,5</sup>  $\text{InAs}_y\text{P}_{1-y}$ ,<sup>6</sup>  $\text{CdSe}_y\text{S}_{1-y}$ ,<sup>7,8</sup> and  $\text{Ge}_y\text{Si}_{1-y}$ .<sup>9</sup> In  $\text{GaAs}_y\text{P}_{1-y}$ , for example, the reflectivity spectrum displays two distinct bands. One band lies at frequencies close to the optical phonon mode of pure GaAs and the other band near the mode frequency of pure GaP. The strength of each band depends upon the composition, the GaAs-like band increasing with  $y$  and the GaP-like band with  $(1-y)$ .

The two-band behavior would have been expected if the second group of crystals consisted of imperfect solid solutions. However, studies of  $\text{GaAs}_y\text{P}_{1-y}$ <sup>4,5</sup> and

$\text{CdSe}_y\text{S}_{1-y}$ <sup>8</sup> using the electron-beam microprobe and x-ray powder spectra showed no large-scale clustering of A, P, Se, or S.

If one compares the infrared-active mode frequencies in crystals of the two groups (i.e., one-band and two-band crystals), one finds in the one-band case that the TO (transverse optic) mode of the lighter ion parent crystals lies between the TO and LO mode frequencies of the heavier-ion parent crystal. In the two-band mixed crystals the TO mode of the lighter ion parent crystal lies well outside this range. This suggests that two bands will only appear in those mixed-crystal systems in which the relevant optical modes of the parent crystals are well separated. Such requirements are known to exist for the appearance of local-mode structure due to impurity atoms.<sup>10</sup> Local-mode theory will be applicable to the mixed crystals for  $y$  close to 0 or 1. For the formation of a local mode in a diatomic host lattice the mass ratio of the host ions to the impurity ions must exceed certain minimum values depending on which host ion the impurity ion replaces.<sup>10</sup> The situation in polar crystals is complicated by the effect of long-range Coulomb forces which are usually neglected in local-mode theories.

A preliminary discussion has been given of the dependence of the mixed-crystal modes on the parameters of the pure crystals using a simple model to illustrate the important concepts.<sup>3</sup> In the present paper the lattice dynamics are treated in detail to include mass- and force-constant changes as well as the local-field corrections. Infrared and Raman spectra are computed from the model for comparison with experiments performed on  $\text{Ba}_y\text{Sr}_{1-y}\text{F}_2$  and  $\text{Sr}_y\text{Ca}_{1-y}\text{F}_2$ .

For the two-band mixed crystals  $\text{GaAs}_y\text{P}_{1-y}$  and  $\text{CdSe}_y\text{S}_{1-y}$  a model of the long-wavelength lattice vibrations was previously developed which allowed us to calculate the infrared- and Raman-mode frequencies and strengths as a function of composition and cluster-

<sup>1</sup> R. K. Chang, B. Lacina, and P. S. Pershan, *Phys. Rev. Letters* **17**, 755 (1966).

<sup>2</sup> P. J. Gielisse, J. N. Plendl, and L. C. Mansur, *J. Appl. Phys.* **36**, 2446 (1965).

<sup>3</sup> A. S. Barker, Jr., and H. W. Verleur, *Solid State Commun.* **5**, 695 (1967).

<sup>4</sup> H. W. Verleur and A. S. Barker, Jr., *Phys. Rev.* **149**, 715 (1966).

<sup>5</sup> Y. S. Chen, W. Shockley, and G. L. Pearson, *Phys. Rev.* **151**, 648 (1966).

<sup>6</sup> F. Oswald, *Z. Naturforsch.* **14A**, 374 (1959).

<sup>7</sup> M. Balkanski, R. Besserman, and J. M. Besson, *Solid State Commun.* **4**, 201 (1966).

<sup>8</sup> H. W. Verleur and A. S. Barker, Jr., *Phys. Rev.* **155**, 750 (1967).

<sup>9</sup> D. W. Feldman, M. Ashkin, and J. H. Parker, Jr., *Phys. Rev. Letters* **17**, 1209 (1966).

<sup>10</sup> S. S. Jaswal, *Phys. Rev.* **137**, 302 (1965).

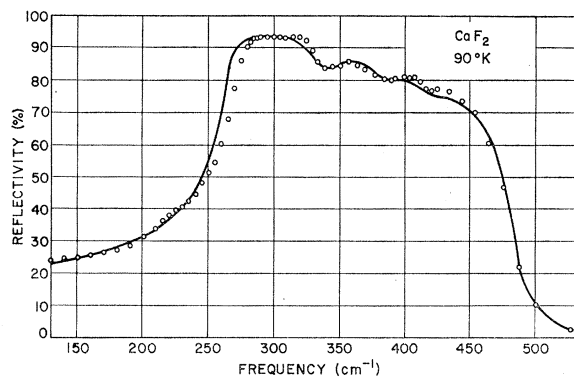


FIG. 1. Reflectivity spectrum of  $\text{CaF}_2$  at  $90^\circ\text{K}$ . Open circles represent experimental data. Solid curve is classical oscillator fit using mode parameters listed in Table I.

ing. This earlier work (Refs. 4 and 8) will be referred to as I and II. The calculations based on the model were in good agreement with the experimental data for these two systems. The essential feature of the model was the recognition of the existence of five basic nearest-neighbor ion complexes or units corresponding to the five possible distinct arrangements of anions around a given cation. A probability argument was used to determine the number of each of these units in the lattice at all values of  $y$ . This probability argument involved the introduction of a cluster parameter  $\beta$  as the simplest one-parameter extension of the random-probability case. In the random case all probabilities are simply combinations of  $y$  and  $(1-y)$ . For  $\text{GaAs}_y\text{P}_{1-y}$  and  $\text{CdSe}_y\text{S}_{1-y}$  the cluster parameter,  $\beta$  resulting from the fits took on positive values, implying a tendency for like anions to cluster around a given cation. Although the values of  $\beta$  chosen to give a best fit markedly affected the structure of the two reststrahlen bands, the existence of two distinct bands did not depend on the value of  $\beta$ .

None of the assumptions underlying the model developed in I were applicable exclusively to  $\text{GaAs}_y\text{P}_{1-y}$  or  $\text{CdSe}_y\text{S}_{1-y}$ . Hence it seemed appropriate to test its applicability to a mixed-crystal system of the one-band type of which  $\text{Ba}_y\text{Sr}_{1-y}\text{F}_2$  and  $\text{Sr}_y\text{Ca}_{1-y}\text{F}_2$  are representative. In order to make comparisons with the experimental work of Chang *et al.*,<sup>1</sup> we have extended the model to yield the Raman-active modes as well as the infrared-active modes.

The linear dependence upon concentration of the frequency of the single Raman mode in  $\text{Ba}_y\text{Sr}_{1-y}\text{F}_2$  and  $\text{Sr}_y\text{Ca}_{1-y}\text{F}_2$  led Chang *et al.* to suggest that a virtual-ion model might be applicable to these mixed crystals.<sup>1,3</sup> Calculations are made below of the Raman- and infrared-mode behavior using the virtual-ion model and comparisons are made with experiment and with our model. It will be seen that both models agree in the prediction of the Raman frequency but that our model yields better agreement with the experimental infrared reflectivity spectra. The virtual-ion model with its one mode fails completely of course when applied to a two-band

crystal like  $\text{GaAs}_y\text{P}_{1-y}$ . Chen *et al.*<sup>4</sup> have recognized the need for more than one degree of freedom in describing the two-band crystal  $\text{GaAs}_y\text{P}_{1-y}$ . They developed a model with two degrees of freedom for the optical modes. Their model, however, cannot account for the fine structure observed in the two distinct reststrahlen bands since these obviously require additional degrees of freedom. The model developed in Refs. 4 and 8 has 12 degrees of freedom for the optical modes, and can predict the main bands and the fine structure in  $\text{GaAs}_y\text{P}_{1-y}$ . The 12 degrees of freedom are suggested by the nearest-neighbor environments. The model is extended here for the fluorite structure which has slightly more complex nearest-neighbor environments since the pure fluorite-type crystals have three ions in a primitive cell compared with two in  $\text{GaAs}$  and  $\text{GaP}$ .

Section II describes the experimental work on the barium, strontium, and calcium fluorides and their mixed crystals. In Secs. III and IV a model is developed for the lattice dynamics of the fluorite structure. This model will predict one- or two-mode behavior depending on the atomic-force parameters. In addition to explaining the observed spectra, examination of the ion displacements given by this model shows under what conditions the virtual-ion model is a good approximation.

## II. EXPERIMENTAL WORK AND RESULTS

### Samples

Three representative samples of both  $\text{Ba}_y\text{Sr}_{1-y}\text{F}_2$  and  $\text{Sr}_y\text{Ca}_{1-y}\text{F}_2$  were purchased from Optovac, Inc. The respective compositions were approximately  $y=0.25$ ,  $0.5$ , and  $0.75$ . The exact composition was determined by x-ray powder diffraction, assuming linear dependence of the lattice constant on concentration. Our observations here agree with those of Chang *et al.*<sup>1</sup> who obtained samples from the same source, in that no evidence was found for deviations from homogeneous solid solutions. It should be realized, however, that x-ray powder measurements are not sensitive to clusters or deviations from random mixtures in regions

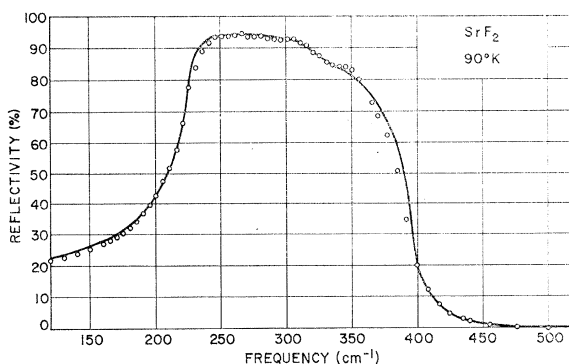


FIG. 2. Reflectivity spectrum of  $\text{SrF}_2$  at  $90^\circ\text{K}$ . Open circles represent experimental data. Solid curve is classical oscillator fit using mode parameters listed in Table I.

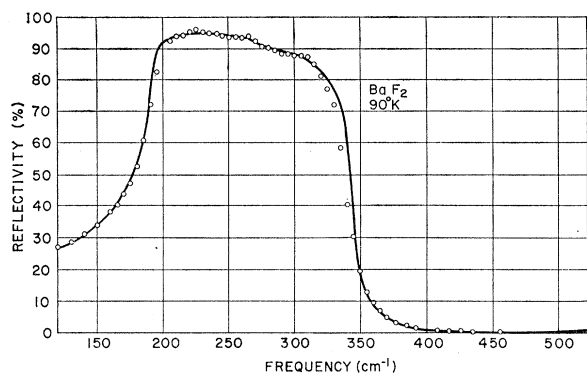


FIG. 3. Reflectivity spectrum of  $\text{BaF}_2$  at  $90^\circ\text{K}$ . Open circles represent experimental data. Solid curve is classical oscillator fit using mode parameters listed in Table I.

extending over only several atomic diameters. Crystals of pure  $\text{BaF}_2$ ,  $\text{SrF}_2$  and  $\text{CaF}_2$  were obtained and included in the x-ray powder analysis to fix the endpoint of the concentration range. Since all crystals are cubic, no special orientation is required for infrared work. The crystals were mechanically lapped, then polished with diamond abrasive to provide a flat, smooth surface at least 4 by 6 mm.

#### Reflectivity Spectra

The infrared reflectivity spectra for unpolarized light at  $15^\circ$  incidence were measured both at 300 and  $90^\circ\text{K}$  over the frequency range from 100 to  $1000\text{ cm}^{-1}$ , using conventional spectrometers. The general method for taking data has been discussed by Spitzer and Kleinman.<sup>11</sup> The spectral slit width was never more than  $2.5\text{ cm}^{-1}$  over the entire frequency range.

#### Pure Crystals

The room-temperature reflectivity spectra of  $\text{CaF}_2$ ,  $\text{SrF}_2$  and  $\text{BaF}_2$  were originally measured by Kaiser *et al.*<sup>12</sup> Our room-temperature measurements are in substantial agreement with these workers' including the observation of a weak mode besides the dominant transverse optic (TO) mode in all three crystals. The experimental reflectivity spectra of the three crystals at  $90^\circ\text{K}$  are shown in Figs. 1, 2, and 3 (open circles). The solid curves in these figures represent classical oscillator fits to these spectra. The mode parameters used to obtain these curves are listed in Table I, together with the corresponding room-temperature values given by Kaiser *et al.*<sup>12</sup>

The origin and temperature dependence of the weak mode is of special interest for the analysis of the mixed crystal spectra carried out below. In all three fluorides, the strength of this mode decreases by a factor of about

six on cooling from 300 to  $90^\circ\text{K}$ . Kaiser *et al.*<sup>12</sup> suggested that this mode is a two-phonon summation band involving the TO mode and an acoustic mode. A calculation of the temperature dependence of the strength of such a mode shows that it should decrease upon cooling from 300 to  $90^\circ\text{K}$  by a factor of only 2.5. On the other hand if this mode is a two-phonon difference band formed from the LO mode and an acoustic mode, the calculated temperature dependence is in close agreement with experiment.

In addition to the strongest combination band discussed above, other very weak high-frequency modes are observed in the reflectivity spectra of these crystals. These modes have not been previously reported. Modes 3 and 4 (Table I) appear as small dips at the high-frequency side of the reststrahlen band of  $\text{CaF}_2$ . The fifth mode corresponds to the rounding of the high-frequency shoulder of the reflectivity peak in this crystal. The same type of mode is listed as the third mode in  $\text{SrF}_2$  and  $\text{BaF}_2$ . We have not assigned these modes but assume that they are due to combination bands.

In all cases the main combination band structure in the reflectivity spectra of  $\text{CaF}_2$ ,  $\text{SrF}_2$  and  $\text{BaF}_2$  is strongly suppressed at  $90^\circ\text{K}$ . To simplify interpretation we shall, therefore, make a detailed analysis of only the low-temperature measurements.

#### Mixed Crystals

The reflectivity spectra of the mixed crystals  $\text{Ba}_y\text{Sr}_{1-y}\text{F}_2$  and  $\text{Sr}_y\text{Ca}_{1-y}\text{F}_2$  were measured both at 300 and at  $90^\circ\text{K}$ . At both temperatures and for both systems the spectra consist of essentially a single reflectivity peak with some fine structure. In Fig. 4 we have shown the  $90^\circ\text{K}$  reflectivity spectra of three mixed crystals of  $\text{Ba}_y\text{Sr}_{1-y}\text{F}_2$  together with the spectra of the pure crystals for comparison. When we come to classical-oscillator fits of these spectra we shall see that some of the fine structure observed in the spectra of the parent crystals continues in the mixed crystals with properly scaled frequencies. However, the pronounced dip in reflectivity which is especially noticeable in the low-temperature spectra and varies with composition from about 260 to  $280\text{ cm}^{-1}$  in  $\text{Ba}_y\text{Sr}_{1-y}\text{F}_2$  and from about 300 to  $330\text{ cm}^{-1}$  in  $\text{Sr}_y\text{Ca}_{1-y}\text{F}_2$ , cannot be traced to any of the weak modes in the parent crystals. Moreover, the strength of this mode is temperature insensitive. We assign this dip to a fundamental mode (or modes) in the mixed crystal.

### III. LONG-WAVELENGTH PHONON VIBRATIONS IN THE $\text{CaF}_2$ STRUCTURE

#### Equations of Motion and Polarization

$\text{CaF}_2$  crystallizes in the fluorite structure with space group  $O_h^5$ . A primitive cell of  $\text{CaF}_2$  is shown in Fig. 5.

<sup>11</sup> W. G. Spitzer and D. A. Kleinman, Phys. Rev. **121**, 1324 (1961).

<sup>12</sup> W. Kaiser, W. G. Spitzer, R. H. Kaiser, and L. E. Howarth, Phys. Rev. **127**, 1950 (1962).

TABLE I. Mode parameters used in classical oscillator fits of parent crystals. Room-temperature data are from Kaiser *et al.* (Ref. 12). 90°K data are from present measurements. Note: Our 300°K measurements yield the values: (a) 261 cm<sup>-1</sup>, (b) 0.033, (c) 0.025 for these mode parameters.

Mode Parameters	CaF		SrF <sub>2</sub>		BaF <sub>2</sub>	
	300°F	90°K	300°K	90°K	300°K	90°K
$\nu_1(\text{TO}) (\text{cm}^{-1})$	257 (a)	265	217	225	184	192
$4\pi\rho_1$	4.2	4.4	4	4.17	4.5	4.7
$\Gamma_1$	0.018 (b)	0.025	0.017 (c)	0.025	0.02	0.025
$\nu_2 (\text{cm}^{-1})$	328	340	316	330	278	280
$4\pi\rho_2$	0.4	0.07	0.07	0.0125	0.07	0.01
$\Gamma_2$	0.35	0.1	0.25	0.15	0.3	0.15
$\nu_3 (\text{cm}^{-1})$		385		370		320
$4\pi\rho_3$		0.02		0.0125		0.005
$\Gamma_3$		0.1		0.2		0.2
$\nu_4 (\text{cm}^{-1})$		420				
$4\pi\rho_4$		0.01				
$\Gamma_4$		0.1				
$\nu_5 (\text{cm}^{-1})$		460				
$4\pi\rho_5$		0.01				
$\Gamma_5$		0.2				
$\nu_{\text{LO}} (\text{cm}^{-1})$	463	474	374	392	326	342
$\nu_{\text{ao}} (\text{cm}^{-1})$	71	134	99	162	94	162
$\epsilon_\infty$	2.045	2.045	2.07	2.07	2.16	2.16
$\epsilon_0 = \epsilon_\infty + \sum 4\pi\rho$	6.65	6.545	6.14	6.26	6.73	6.87

It contains one formula unit, that is two F ions (F<sub>1</sub> and F<sub>2</sub>), and one Ca ion. BaF<sub>2</sub> and SrF<sub>2</sub> have the same structure as CaF<sub>2</sub>, hence the forms of the equations developed below are identical for these crystals.

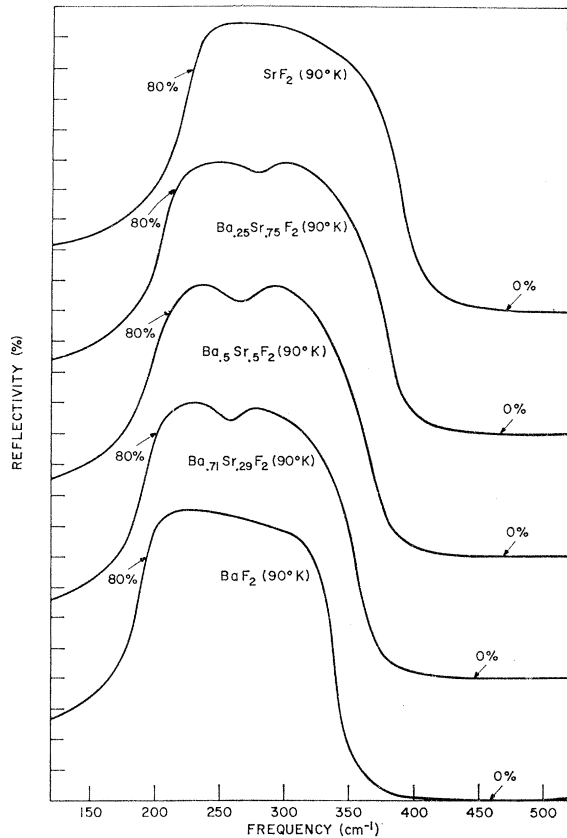


FIG. 4. Comparison of experimental reflectivity spectra at 90°K of the pure crystals BaF<sub>2</sub> and SrF<sub>2</sub> with three mixed crystals of Ba<sub>y</sub>Sr<sub>1-y</sub>F<sub>2</sub>.

Group character analysis of the long-wavelength ( $q \approx 0$ ) lattice vibrations shows that the phonon dispersion curves consist of three acoustic branches and six optic branches. At  $q \approx 0$  three of the latter are infrared-active modes of vibration (one doubly degenerate TO mode and one LO mode). The remaining three optic modes are Raman active and triply degenerate. Following the procedure outlined by Born and Huang,<sup>13</sup> using the polarizable-ion model, we can write equations of motion for the three ions in the primitive cell. Since the structure is cubic, the dielectric function connected with the infrared modes is isotropic and there are no preferred directions for measuring infrared spectra. For simplicity we write scalar equations and choose the vibration direction along the line joining the fluorine ions F<sub>1</sub> and F<sub>2</sub> (see Fig. 5). In the harmonic approximation we write

$$m_F \ddot{w}_{F1} = +k_1(w_{Ca} - w_{F1}) + k_6(w_{F2} - w_{F1}) - \frac{1}{2}eE_{\text{eff}}, \quad (1)$$

$$m_F \ddot{w}_{F2} = +k_1(w_{Ca} - w_{F2}) + k_6(w_{F1} - w_{F2}) - \frac{1}{2}eE_{\text{eff}}, \quad (2)$$

$$m_{Ca} \ddot{w}_{Ca} = k_1(w_{F1} - w_{Ca}) + k_1(w_{F2} - w_{Ca}) + eE_{\text{eff}}. \quad (3)$$

The  $m$ 's are the ionic masses, the  $w$ 's ionic displacements;  $k_1$  is the nearest-neighbor force constant between F and Ca ions,  $k_6$  the second-neighbor force constant between F<sub>1</sub> and F<sub>2</sub>,  $E_{\text{eff}}$  is the effective electric field which acts on the effective ionic charges  $-\frac{1}{2}e$  and  $+e$  of the F and Ca ions, respectively. No second-neighbor force appears in Eq. (3) since the second neighbors of a Ca ion are 12 Ca ions which must all be moving in unison with it for a  $q \approx 0$  vibration.

As we did in the development of the model for GaAs<sub>y</sub>P<sub>1-y</sub> in I, we approximate the partial overlap of the electron cloud around each ion with adjacent cells

<sup>13</sup> M. Born and K. Huang, *Dynamical Theory of Crystal Lattices* (Clarendon Press, Oxford, England, 1954).

by dividing the effective ionic charge  $e$  into a local and nonlocal portion:

$$e = e_{\text{loc}} + e_{\text{n1}}. \quad (4)$$

The nonlocal part represents the overlapping part of  $e$  which extends outside the cell and experiences the macroscopic field  $E$ , rather than  $E_{\text{eff}}$ . Since these fluorides are much more ionic than the III-V and II-VI compounds analyzed previously, we expect the nonlocal portion to be much smaller than the local part of the total effective ionic charge.

With this assumption concerning the charge distribution and taking the cubic symmetry of the crystal into account, we obtain for the effective field acting on the local charges:

$$E_{\text{eff}} = E + \frac{4}{3}\pi P_{\text{loc}}. \quad (5)$$

$E$  is the macroscopic electric field and  $P_{\text{loc}}$  is the atomic displacement polarization given by:

$$P_{\text{loc}} = Ne_{\text{loc}}(w_{\text{Ca}} - \frac{1}{2}w_{\text{F1}} - \frac{1}{2}w_{\text{F2}}). \quad (6)$$

$N$  is the number of molecules per unit volume, i.e., the reciprocal of the primitive cell volume.

The total polarization is

$$P = N(e_{\text{loc}} + e_{\text{n1}})(w_{\text{Ca}} - \frac{1}{2}w_{\text{F1}} - \frac{1}{2}w_{\text{F2}}) + N(\alpha_{\text{F1}} + \alpha_{\text{F2}} + \alpha_{\text{Ca}})E. \quad (7)$$

The first term arises from the ion motion creating a dipole proportional to  $e$ . The second term is the electronic polarization with the polarizabilities of the ions given by the  $\alpha$ 's. We have assumed that the electronic polarization effects can be related to the macroscopic field  $E$ , i.e., that the local-field correction can be included by using Eq. (7) and treating the  $\alpha$ 's as effective polarizabilities.

We now substitute for the effective field in Eqs. (1), (2), and (3) from Eqs. (5) and (6). Assuming that  $P$ ,  $E$ , and the displacements have  $\exp(i\omega t)$  time dependence, the three linear equations are solved for the eigenfrequencies and eigenvectors of the normal vibrations. The solutions are listed in Table II.

The first mode, where all ions move together is the acoustic mode. The relative displacement of the Ca sublattice against the two F sublattices moving in unison, typifies the second mode as the infrared-active mode. For the third normal mode, which is Raman active, the two F sublattices move against each other, while the Ca sublattice is stationary.

We note in passing that the second-neighbor force constant  $k_6$  between  $F_1$  and  $F_2$  appears only in the Raman frequency, since in the infrared-active mode the two F sublattices are not relatively displaced. The second-neighbor force constant between the Ca ions does not appear in the equations of motion since these ions do not move relative to each other at  $\mathbf{q} = 0$ .

TABLE II. Eigenfrequencies and Eigenvectors of normal vibrations in  $\text{CaF}_2$  structure.

Mode	Frequency	Displacements corresponding to Eigenvectors of Eqs. (1)-(3)
Acoustic	$\omega_{\text{acc}}^2 = 0$	$w_{\text{F1}} = w_{\text{F2}} = w_{\text{Ca}}$
I.R.	$\omega_{\text{TO}}^2 = \frac{2k_1 - 4\pi N e_{\text{loc}}^2}{\bar{m}_{\text{CaF2}}}$	$w_{\text{F1}} = w_{\text{F2}}; w_{\text{Ca}} = -\frac{2m_{\text{F}}}{m_{\text{Ca}}}w_{\text{F1}}$
Raman	$\omega_{\text{R}}^2 = \frac{(k_1 + 2k_6)}{m_{\text{F}}}$	$w_{\text{F1}} = -w_{\text{F2}}; w_{\text{Ca}} = 0$ $\left( \bar{m}_{\text{CaF2}} = \frac{2m_{\text{F}}m_{\text{Ca}}}{2m_{\text{F}} + m_{\text{Ca}}} \right)$

### Infrared Mode Strength

To obtain the classical oscillator strength of the infrared-active mode we evaluate the dielectric function  $\epsilon(\omega)$  from the definition

$$P = \frac{\epsilon(\omega) - 1}{4\pi} E. \quad (8)$$

Substituting for  $w$  and  $E$  in Eq. (7) and combining with Eq. (8) we obtain

$$\epsilon(\omega) = \epsilon_{\infty} + \frac{4\pi N e^2 / \bar{m}_{\text{CaF2}}}{(\omega_{\text{TO}}^2 - \omega^2 - i\Gamma\omega\omega_{\text{TO}})}. \quad (9)$$

The term in the resonant denominator proportional to  $\Gamma$  has been added to represent the effect of damping. The classical oscillator strength ( $4\pi\rho$ ) is given by the difference between the low- and the high-frequency dielectric constants.

$$4\pi\rho \equiv \epsilon_0 - \epsilon_{\infty} = 4\pi N e^2 / \bar{m}_{\text{CaF2}} \omega_{\text{TO}}^2. \quad (10)$$

### Raman Mode Strength

The ion motions considered in writing Eqs. (1) to (3) were along the line joining  $F_1$  and  $F_2$ . We can choose the

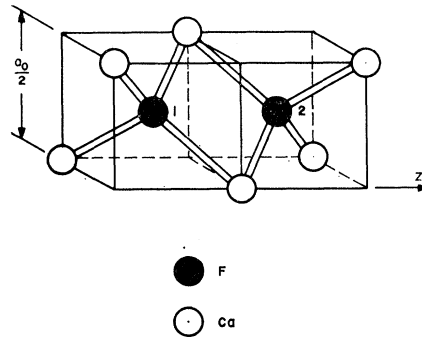


FIG. 5. Primitive cell of  $\text{CaF}_2$  structure. The primitive cell contains two F ions at the center of two tetrahedra. The relation of the standard x-ray cell length  $a_0$  to this primitive cell is shown.

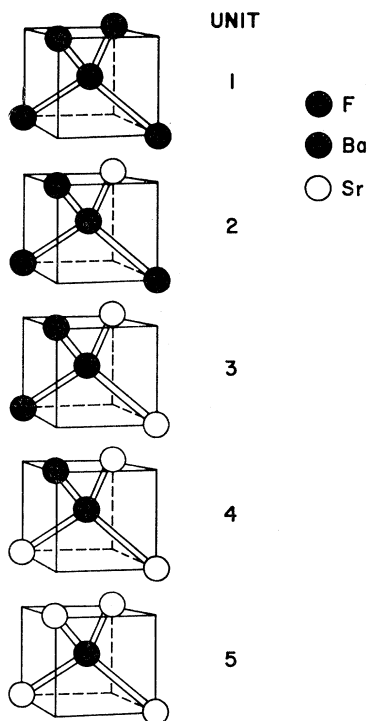


FIG. 6. Basic units of nearest-neighbor ions around a F ion site. Units 2, 3, and 4 must occur in other orientations besides those pictured here to agree with the observed optical isotropy of the crystals.

$z$  axis (Fig. 5) along this direction. Testing the Raman mode listed in Table II under the point-group operations in  $O_h$  shows that it belongs to the threefold degenerate representation  $T_{2g}$ . Since second-order tensors with components  $\alpha_{xy}$ ,  $\alpha_{xz}$ ,  $\alpha_{yz}$  transform under  $T_{2g}$  we readily identify the mode we have derived in Table I as a Raman-active (and infrared-inactive) mode producing polarizability  $\alpha_{xy}$ . Two other orthogonal (but degenerate) Raman modes may be chosen with the fluorine ions vibrating along the  $x$  or the  $y$  axes; these will cause polarizabilities  $\alpha_{yz}$  and  $\alpha_{xz}$ , respectively. We write for the electronic polarization

$$\mathbf{P}_{el} = \alpha \cdot \mathbf{E}. \quad (11)$$

Carrying out the usual expansion of  $\alpha$  to first order in the phonon coordinates and assuming that only the  $z$ -directed Raman mode is excited we obtain

$$\alpha = \alpha_{F1} + \alpha_{F2} + \alpha_{Ca} + \alpha^z(w_{F1} - w_{F2}).$$

The symmetry dictates that  $w_{Ca}$  cannot appear and that the F ion displacements must enter as a difference. The first three tensors are diagonal and have been used already in Eq. (7).  $\alpha^z$  has nonzero elements  $\alpha_{xy}^z = \alpha_{yz}^x$  for the mode we wish to consider. Substituting the above expression for  $\alpha$  into Eq. (11) and retaining only the terms which depend on the phonon amplitude we obtain

$$\mathbf{P} = \{\alpha^z(w_{F1} - w_{F2})\} \cdot \mathbf{E}. \quad (12)$$

In a typical Raman experiment the crystal is illumi-

nated with a laser beam whose electric field has time dependence  $\mathbf{E} = \mathbf{E}_0 e^{i\omega t}$ . If  $w_{F1}$  and  $w_{F2}$  are thermally excited and vibrating with frequency  $\omega_R$ , the spectrum of  $P$  will have sidebands at  $\omega_l \pm \omega_R$ . The power in these Raman lines or sidebands per unit power in the laser beam is proportional to  $|\mathbf{P}|^2/|\mathbf{E}_0|^2$ . We define a Raman scattering strength  $A$  corresponding to this latter ratio

$$A = \langle [\alpha_{xy}^z(w_{F1} - w_{F2})]^2 \rangle, \quad (13)$$

where  $\langle \rangle$  denote the thermal average over initial states of the system. The correct result for the Stokes-Raman intensity is obtained by considering the laser mode to lose one quantum, and the Stokes mode (at  $\omega_l - \omega_R$ ) to gain one quantum.<sup>14</sup> Taking the thermal average we obtain for the Stokes line strength

$$A = \frac{2(\alpha_{xy}^z)^2}{m_F} \frac{\hbar}{\omega_R} (N_R + 1), \quad (14)$$

where  $N_R$  is the Bose population factor corresponding to the phonon frequency  $\omega_R$ .<sup>14</sup> For the anti-Stokes line,  $N_R + 1$  is replaced by  $N_R$ .<sup>14,15</sup> For the infrared lattice vibration  $w_{F1} = w_{F2}$  so  $A = 0$  as expected.

To make the connection with more standard forms for the Raman scattering intensity we note that  $\sqrt{A}$  is actually a polarizability. The incident-laser beam creates oscillating dipoles at frequency  $\omega_l - \omega_R$  (for the Stokes case) with dipole moment  $p = (\sqrt{A}E)/N$ . The power radiated by a single dipole of strength  $p$  into solid angle  $d\Omega$  at right angles to the polarization is

$$p^2(\omega_l - \omega_R)^4 d\Omega / (8\pi c^3).$$

We find that the Raman power scattered into solid angle  $d\Omega$  per unit power in the incident laser beam for a crystal of length  $L$  is

$$S = \frac{A(\omega_l - \omega_R)^4 L d\Omega}{2Nc^4}. \quad (15)$$

We thus obtain the familiar fourth power of frequency, and the linear length dependence.<sup>15</sup>  $N$  may be combined with the ion mass contained in  $A$  [Eq. (14)] to give the density factor which is often quoted in formulas for the Raman scattering efficiency. For simplicity, in the calculations which follow we compute  $A$  from Eq. (14) (i.e., the geometry-independent part of  $S$ ) and call this the Raman mode strength.

#### Determination of Atomic Parameters

The reflectivity at normal incidence is related to the dielectric constant by the Fresnel equation:

$$R = \left| \frac{[\epsilon(\omega)]^{1/2} - 1}{[\epsilon(\omega)]^{1/2} + 1} \right|^2. \quad (16)$$

<sup>14</sup> G. Placzek, *Handbuch der Radiologie* (Akademische Verlagsgesellschaft, VI, Leipzig, 1934), Vol. 2, p. 209. Translation available from Department of Commerce, Washington, D. C.

<sup>15</sup> R. Loudon, *Advan. Phys.* **13**, 423 (1964).

Fits of this calculated reflectivity to experimental spectra allow us to determine the mode parameters  $\epsilon_\infty$ ,  $\omega_{TO}$ ,  $4\pi\rho$ , and  $\Gamma$  which enter  $\epsilon(\omega)$  [see Eq. (9)]. The fitting procedure has been discussed in the literature.<sup>11</sup> Once the mode parameters are known we can calculate the total effective ionic charge from Eq. (10) since  $N$  is known from the x-ray cell size. In addition the expressions for the  $\mathbf{q}=0$  infrared TO and Raman mode frequencies give us two equations for the three atomic parameters  $k_1$ ,  $k_6$ , and  $e_{loc}$ . Individual values for these latter parameters will be obtained only when we apply our model to the mixed-crystal reflectivity spectra since we then obtain additional relations between the three constants. Measurements of the strength of the Raman mode allow the determination of the atomic parameter  $\alpha_{xy}^2$ . Such measurements have not been carried out by the present authors; however calculated results are presented for the Raman mode strength assuming  $\alpha_{xy}^2$  is the same in all three fluorides. The Raman modes in  $\text{BaF}_2$ ,  $\text{SrF}_2$ , and  $\text{CaF}_2$  will not have the same strengths of course because of the factors  $(N+1)$  and  $\omega_R$  appearing in Eq. (14). Values of  $A$  for the pure and mixed crystals are presented below.

#### IV. APPLICATION OF THE MIXED-CRYSTAL MODEL TO $\text{Ba}_y\text{Sr}_{1-y}\text{F}_2$ AND $\text{Sr}_y\text{Ca}_{1-y}\text{F}_2$

##### Basic Units and Their Probability of Occurrence

Examination of Fig. 5 shows that the four nearest neighbors of either an  $\text{F}_1$  or an  $\text{F}_2$  ion in pure  $\text{CaF}_2$  are Ca ions arranged at the corners of a tetrahedron. These four cation positions in a mixed crystal of  $\text{Ba}_y\text{Sr}_{1-y}\text{F}_2$ , may be occupied by either Ba or Sr ions. The situation is quite similar to the one considered in I: For each of the F ions in a unit cell there are five possible distinct nearest-neighbor environments, which we call basic units. They are shown in Fig. 6. Because we must distinguish between the two F ions in order to properly describe the Raman-active modes, we will consider ten basic units (rather than five, as was done in I), five for each of the two F ions. The mixed crystal is considered to be built up from these ten basic units.

The probabilities of finding a Ba ion next to a Ba ion and a Sr ion next to a Sr ion are given by

$$P_{\text{BaBa}} = y + \beta(1-y), \quad (17)$$

$$P_{\text{SrSr}} = (1-y) + \beta y. \quad (18)$$

These equations are identical with Eqs. (1) and (2) in I with different subscripts. Since five types of nearest-neighbor environments are possible we might expect that up to five parameters could be introduced in the probability expressions. The introduction of  $\beta$  represents the simplest improvement over the random-probability case. We call  $\beta$  the clustering (or disorder) parameter. If  $\beta$  is positive (but smaller than or equal to one), the probability of finding a Ba ion next to another Ba ion is enhanced over the random case where  $\beta=0$ . This type

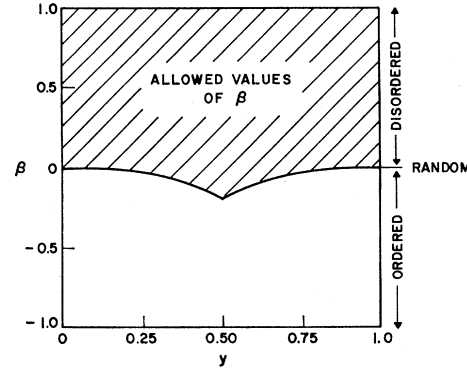


FIG. 7. Allowed values for  $\beta$  as a function of  $y$ .

of disorder (i.e., positive values of  $\beta$ ) was found to exist in  $\text{GaAs}_y\text{P}_{1-y}$  and also in  $\text{CdSe}_y\text{S}_{1-y}$ , although in different degrees.

If order exists in the crystal, i.e., if Ba ions are preferentially surrounded by Sr ions and vice versa,  $\beta$  will take on negative values. For example in a one-dimensional crystal, the completely ordered situation for a 50-50 alloy would be  $\text{BaSrBaSr} \dots$ . For this ordered crystal we would have

$$P_{\text{BaBa}}=0, \quad P_{\text{BaSr}}=1,$$

$$P_{\text{SrSr}}=0, \quad P_{\text{SrBa}}=1,$$

which corresponds to  $\beta=-1$ . At other compositions  $\beta$  must have minimum values larger than  $-1$  to prevent the probabilities from becoming negative.

For the present case, as in I, we use Eqs. (17) and (18) to calculate the probabilities of occurrence  $f_i$  of units of type  $i$  (see Fig. 6). In terms of the basic probabilities given in Eqs. (17) and (18) the probabilities of occurrence of these basic units are<sup>4</sup>:

$$f_1 = y(P_{\text{BaBa}} - y + yP_{\text{BaBa}}^2), \quad (19)$$

$$f_2 = 4y^2(1 - P_{\text{BaBa}})P_{\text{BaBa}}, \quad (20)$$

$$f_3 = 6y^2(1 - P_{\text{BaBa}})^2, \quad (21)$$

$$f_4 = 4(1-y)^2P_{\text{SrSr}}(1 - P_{\text{SrSr}}), \quad (22)$$

$$f_5 = (1-y)[P_{\text{SrSr}} - 1 + y + (1-y)P_{\text{SrSr}}^2]. \quad (23)$$

Only those values of  $\beta$  are admissible for which all of the probabilities Eqs. (19) to (23) are positive. The range of allowed values for  $\beta$  is shown in Fig. 7 for all  $y$ .

##### Equations of Motion and Polarization

The only formal difference between the two systems considered here and the  $\text{GaAs}_y\text{P}_{1-y}$  model developed in I arises from the introduction of a total of ten F sublattice coordinates, rather than five. We have in fact five  $\text{F}_1$  sublattice coordinates  $w_{\text{F}_1}(i)$ ,  $i=1$  to 5, and five  $\text{F}_2$  sublattice coordinates  $w_{\text{F}_2}(i)$ ,  $i=1$  to 5, to take account of the five possible nearest-neighbor environments of each of the F ions. For the cations, however,

we have  $w_{\text{Ba}}(i)$ ,  $i=1$  to 4, and  $w_{\text{Sr}}(i)$ ,  $i=2$  to 5, for the  $\text{Ba}_y\text{Sr}_{1-y}\text{F}_2$  system and  $w_{\text{Sr}}(i)$ ,  $i=1$  to 4, and  $w_{\text{Ca}}(i)$ ,  $i=2$  to 5 for the  $\text{Sr}_y\text{Ca}_{1-y}\text{F}_2$  system. These coordinates are exactly like the anion coordinates used in I. In spite of the large number of coordinates or degrees of freedom (eighteen) in this model we will find below that there are

actually fewer parameters (force constants and charges) than were used for the mixed crystals described in Refs. 4 and 8.

Using again  $\text{Ba}_y\text{Sr}_{1-y}\text{F}_2$  as an example, the equations of motion, corresponding to Eqs. (13), (14), and (15) of I are

$$\begin{aligned} x(i)f_im_{\text{Ba}}\ddot{w}_{\text{Ba}}(i) = & +x(i)f_ik_1(i)[w_{\text{F1}}(i)+w_{\text{F2}}(i)-2w_{\text{Ba}}(i)] \\ & +x(i)f_ik_7\sum_{j=1}^5 f_j[w_{\text{F1}}(j)+w_{\text{F2}}(j)-2w_{\text{Ba}}(i)]+x(i)f_ik_3\sum_{j=1}^5 x(j)f_j[w_{\text{Ba}}(j)-w_{\text{Ba}}(i)] \\ & +x(i)f_ik_4\sum_{j=1}^5 [1-x(j)]f_j[w_{\text{Sr}}(j)-w_{\text{Ba}}(i)]+x(i)f_ie_{\text{Ba}}E_{\text{eff}}, \quad (24) \end{aligned}$$

$$\begin{aligned} [1-x(i)]f_im_{\text{Sr}}\ddot{w}_{\text{Sr}}(i) = & +[1-x(i)]f_ik_2(i)[w_{\text{F1}}(i)+w_{\text{F2}}(i)-2w_{\text{Sr}}(i)] \\ & +[1-x(i)]f_ik_8\sum_{j=1}^5 f_j[w_{\text{F1}}(j)+w_{\text{F2}}(j)-2w_{\text{Sr}}(i)]+[1-x(i)]f_ik_4\sum_{j=1}^5 x(j)f_j[w_{\text{Ba}}(j)-w_{\text{Sr}}(i)] \\ & +[1-x(i)]f_ik_5\sum_{j=1}^5 [1-x(j)]f_j[w_{\text{Sr}}(j)-w_{\text{Sr}}(i)]+[1-x(i)]f_ie_{\text{Sr}}E_{\text{eff}}, \quad (25) \end{aligned}$$

$$\begin{aligned} f_im_{\text{F}}\ddot{w}_{\text{F1}}(i) = & +x(i)f_ik_1(i)[w_{\text{Ba}}(i)-w_{\text{F1}}(i)]+[1-x(i)]f_ik_2(i)[w_{\text{Sr}}(i)-w_{\text{F1}}(i)] \\ & +f_ik_7\sum_{j=1}^5 x(j)f_j[w_{\text{Ba}}(j)-w_{\text{F1}}(i)]+f_ik_8\sum_{j=1}^5 [1-x(j)]f_j[w_{\text{Sr}}(j)-w_{\text{F1}}(i)] \\ & +f_ik_6\sum_{j=1}^5 f_j[w_{\text{F2}}(j)-w_{\text{F1}}(i)]-\frac{1}{2}f_i\{x(i)e_{\text{Ba}}+[1-x(i)]e_{\text{Sr}}\}E_{\text{eff}}, \quad (26) \end{aligned}$$

$$f_im_{\text{F}}\ddot{w}_{\text{F2}}(i) = \text{same as Eq. (26) with } w_{\text{F1}} \text{ and } w_{\text{F2}} \text{ interchanged.} \quad (27)$$

In these equations, the fractional coefficients  $x(i)$  take on the values 1,  $\frac{3}{4}$ ,  $\frac{1}{2}$ ,  $\frac{1}{4}$ , and 0, as  $i$ , the index specifying the unit, goes from 1 to 5. If there are  $N$  "molecules"  $\text{Ba}_y\text{Sr}_{1-y}\text{F}_2$  in the lattice, there are  $x(i)f_iN\text{Ba}$  ions belonging to unit  $i$ . We use force constants out to second neighbors. In unit  $i$ ,  $k_1(i)$  and  $k_2(i)$  are the nearest neighbor Ba-F and Sr-F force constants, respectively. The second-neighbor force constants are  $k_3$  between Ba-Ba,  $k_4$  between Ba-Sr,  $k_5$  between Sr-Sr and  $k_6$  between F<sub>1</sub>-F<sub>2</sub>. Finally, nearest-neighbor forces between the F ions in a unit  $i$  and Ba and Sr ions in surrounding units  $j$  are taken account of by  $k_7$  and  $k_8$ .

We thus have a total of 18 equations, which can be solved as was done in I for the eigenfrequencies and normal modes of the model. Besides the acoustic mode and the 12 infrared-active modes we obtain an additional five Raman-active infrared-inactive modes which were not present in I.

As was done in Sec. III for the pure crystals, we divide the total effective ionic charge into a local and nonlocal portion<sup>4</sup>:

$$\begin{aligned} e_{\text{Ba}} &= e_{\text{Ba,loc}} + e_{\text{Ba,nl}}, \\ e_{\text{Sr}} &= e_{\text{Sr,loc}} + e_{\text{Sr,nl}}. \end{aligned}$$

For the effective charge on the F ions of unit  $i$  we take that linear combination of  $e_{\text{Ba}}$  and  $e_{\text{Sr}}$  which makes the

unit neutral:

$$e_{\text{F1}} = e_{\text{F2}} = -\frac{1}{2}\{x(i)e_{\text{Ba}}+[1-x(i)]e_{\text{Sr}}\}.$$

For the polarization we write an expression similar to Eq. (17) of I which is the appropriate generalization of Eq. (7) used in the present paper for the pure crystals.

$$\begin{aligned} P = N \sum_{j=1}^5 f_j \{ & -\frac{1}{2}\{x(j)e_{\text{Ba}}+[1-x(j)]e_{\text{Sr}}\} \\ & \times [w_{\text{F1}}+w_{\text{F2}}]+x(j)e_{\text{Ba}}w_{\text{Ba}}(j) \\ & +[1-x(j)]e_{\text{Sr}}w_{\text{Sr}}(j)\} + N\alpha E. \quad (28) \end{aligned}$$

Corresponding to Eq. (6), we write

$$\begin{aligned} P_{\text{loc}} = N \sum_{j=1}^5 f_j \{ & -\frac{1}{2}\{x(j)e_{\text{Ba,loc}}+[1-x(j)]e_{\text{Sr,l}}\} \\ & \times [w_{\text{F1}}(j)+w_{\text{F2}}(j)]+x(j)e_{\text{Ba,loc}}w_{\text{Ba}}(j) \\ & +[1-x(j)]e_{\text{Sr,loc}}w_{\text{Sr}}(j)\} \quad (29) \end{aligned}$$

for the polarization due to the local charge in the mixed crystal.



### Theoretical Fit of Reflectivity Spectra

Using Eq. (8) we can solve for the dielectric constant from Eq. (28). The details of this procedure are discussed in the Appendix of I. Since the Raman-active modes have no infrared strength, they do not contribute to the dielectric constant. Consequently, the expression for  $\epsilon$  becomes formally identical with Eq. (A11) of I:

$$\epsilon(\omega, \gamma, \beta) = \epsilon_\infty + \sum_{j=1}^{12} \frac{4\pi\rho_j\omega_j^2}{\omega_j^2 - \omega^2 - i\omega_j\Gamma_j\omega}, \quad (30)$$

where the dependence of  $\epsilon$  on  $\omega$ ,  $\gamma$  and  $\beta$  through the mode parameters has been explicitly indicated. The reflectivity is finally calculated from Eq. (16).

It is interesting to note that even though we have extended the model from 13 to 18 modes, this does not result in a larger number of unknown parameters which must be fitted. The reason for this is that even though we distinguish between the two types of F ions, their surroundings are identical except for a 90° rotation. Hence the same set of nearest-neighbor and second-neighbor force constants link both kinds of F ions to surrounding ions. In fact additional requirements are now to be fulfilled with the same set of parameters. These are the known Raman frequencies of the parent and mixed crystals which must be predicted by the model.

The fitting procedure again consisted of choosing trial parameters for the unknown force constants, local charges and for  $\beta$ ; the calculation of the reflectivity spectrum with these parameters at a particular composition; then adjustment of the parameters and recalculation of the reflectivity until a best fit is obtained. The success of this procedure depends on whether after obtaining a good fit at one composition an adequate fit is also obtained with the same set of parameters at the other compositions. Finally in the case of these two systems, the agreement of the calculated Raman frequencies with the experimental results provided an additional check on the values chosen for the unknown parameters.

TABLE III. Known physical constants used in the calculations of the model.

	Constant	Value
Mass	$m_F$	$3.15 \times 10^{-23}$ g
	$m_{Ca}$	$6.65 \times 10^{-23}$ g
	$m_{Sr}$	$14.54 \times 10^{-23}$ g
	$m_{Ba}$	$22.80 \times 10^{-23}$ g
Charge	$e_{Ca}$	$10.93 \times 10^{-10}$ esu
	$e_{Sr}$	$11.35 \times 10^{-10}$ esu
	$e_{Ba}$	$12.0 \times 10^{-10}$ esu
	$a_0$ (CaF <sub>2</sub> )	5.46 Å
Lattice constant	$a_0$ (SrF <sub>2</sub> )	5.8 Å
	$a_0$ (BaF <sub>2</sub> )	6.2 Å
No. of molecules per unit volume	$N$ (CaF <sub>2</sub> )	$2.45 \times 10^{22}$ /cm <sup>3</sup>
	$N$ (SrF <sub>2</sub> )	$2.0 \times 10^{22}$ /cm <sup>3</sup>
	$N$ (BaF <sub>2</sub> )	$1.68 \times 10^{22}$ /cm <sup>3</sup>

TABLE IV. Force constants and charges determined by the reflectivity curve fitting.

Nearest-neighbor force constants (10 <sup>4</sup> g/sec <sup>2</sup> )				
Symbol	Ba <sub>y</sub> Sr <sub>1-y</sub> F <sub>2</sub>		Sr <sub>y</sub> Ca <sub>1-y</sub> F <sub>2</sub>	
	Ba-F Force constant	Sr-F Force constant	Sr-F Force constant	Ca-F Force constant
$k_1(1)$	3.3		5.0	
$k_1(2)$	3.8		5.45	
$k_1(3)$	4.3		5.9	
$k_1(4)$	4.5		6.35	
$k_2(2)$		2.5		3.0
$k_2(3)$		3.0		3.5
$k_2(4)$		3.5		4.0
$k_2(5)$		4.3		4.5
$k_7$	2.5		1.8	
$k_8$		2.5		2.5
Second-neighbor force constants (10 <sup>4</sup> g/sec <sup>2</sup> )				
Symbol	Between atoms	CaF <sub>2</sub>	SrF <sub>2</sub>	BaF <sub>2</sub>
$k_6$	F <sub>1</sub> -F <sub>2</sub>	2.4	1.3	0.5
$k_3, k_4, k_5$	cation-cation	0.0 ± 0.5	0.0 ± 0.5	0.0 ± 0.5
Local effective ionic charges (esu)				
	$e_{Ca, loc}$	$7.6 \times 10^{-10}$		
	$e_{Sr, loc}$	$8.1 \times 10^{-10}$		
	$e_{Ba, loc}$	$8.5 \times 10^{-10}$		

In Table III, we have listed the physical constants that were known or could be calculated from the known classical oscillator strengths of the parent crystals. Since no data were available on the lattice constants at 90°K, we have used the 300°K values of  $a_0$ . We estimate that  $a_0$  decreases about 0.4% on cooling to 90°K, so the effect on the other atomic parameters is expected to be small.

In Table IV we present the force constants and charges which were determined by curve fitting. We note a considerable difference in the Sr-F force constants depending on whether Sr is the lighter or heavier cation. Of course at the endpoints of the composition range where we have pure SrF<sub>2</sub> in the two systems, the Sr-F force constants must be the same [i.e.,  $k_1(1) + k_7$  in Sr<sub>y</sub>Ca<sub>1-y</sub>F<sub>2</sub> must equal  $k_2(5) + k_8$  in Ba<sub>y</sub>Sr<sub>1-y</sub>F<sub>2</sub>].

The second-neighbor force constants  $k_6$  between F<sub>1</sub> and F<sub>2</sub> are, as expected, somewhat different in the three parent crystals. In the mixed crystals we have assumed a smooth composition-dependent transition from one endpoint value to the other:

$$k_6(\text{Ba}_y\text{Sr}_{1-y}\text{F}_2) = yk_6(\text{BaF}_2) + (1-y)k_6(\text{SrF}_2).$$

The values of the second-neighbor force constants  $k_3$ ,  $k_4$ , and  $k_5$  are expected to be smaller than  $k_6$  since the distance between the cations is  $\sqrt{2}$  times the distance between F<sub>1</sub> and F<sub>2</sub> ions. In the dynamical matrix these force constants appear with small reciprocal mass factors (e.g.,  $k_3/m_{Ba}$ ) because of the relatively large masses of the cations. These two effects suppress the effect of second-neighbor cation-cation interactions. As a result of these effects none of the fits were sensitive to values as large as  $\pm 0.5 \times 10^4$  for these force constants.

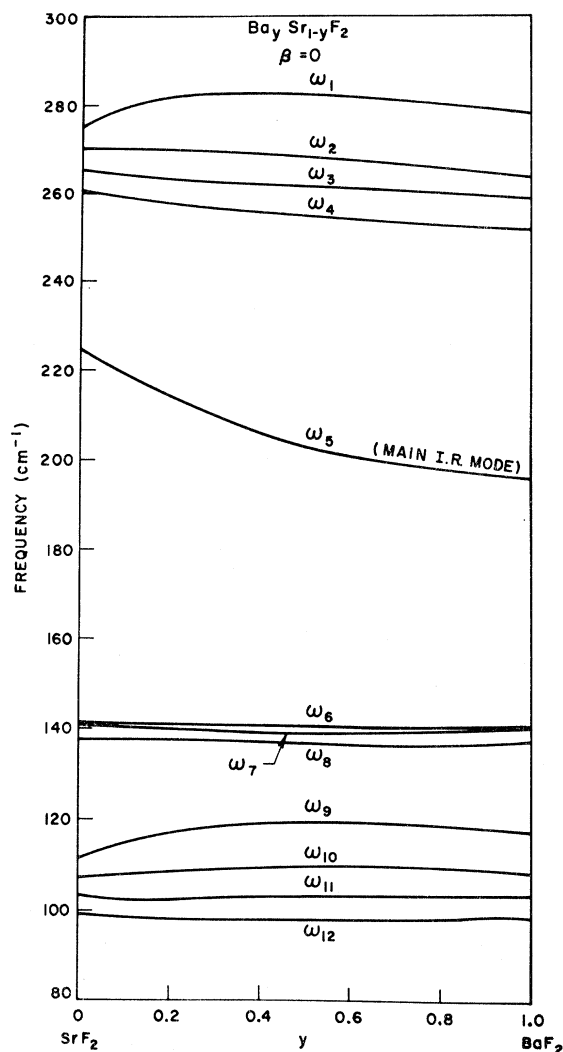


FIG. 8. Infrared-active mode frequencies for  $\text{Ba}_y\text{Sr}_{1-y}\text{F}_2$  versus composition ( $y$ ) computed from the model for  $\beta=0$ . In this and succeeding figures the model is evaluated for  $T=90^\circ\text{K}$ .

In our best fits all cation-cation second-neighbor force constants were set equal to zero. Except at  $y=0.50$  the value of  $\beta$  was found to be zero. Fits were noticeably degraded by choosing  $\beta$  outside the range  $-0.1$  to  $+0.1$ , which is a result in marked contrast to the  $\text{GaAs}_y\text{P}_{1-y}$  system in I. For that crystal system the fits required  $\beta$  values near  $+0.7$  over most of the composition range.

From Table IV we see that the local charges form much larger fractions of the total effective ionic charges (about 70%), than was the case with the III-V and II-VI compounds. This behavior agrees with the usual classification of these fluorides as ionic compounds.

In Figs. 8 and 9 we have plotted the frequencies of the 12 infrared-active modes of the mixed crystals as functions of composition for  $\beta=0$ . Besides the main infrared (I.R.) mode there are three groups of modes with rather closely spaced frequencies. We have plotted the oscillator strengths of the main mode and of the

three groups for both mixed-crystal systems in Figs. 10 and 11. As in I and II the clustering parameter  $\beta$  has little effect on the mode frequencies (Figs. 8 and 9) but a large effect on the mode strengths. The principal effect of choosing  $\beta=-0.15$  is to lower the strength curve for modes 1-4 in Figs. 10 and 11. The curves are lowered about a factor of two near  $y=0.5$ . Negative

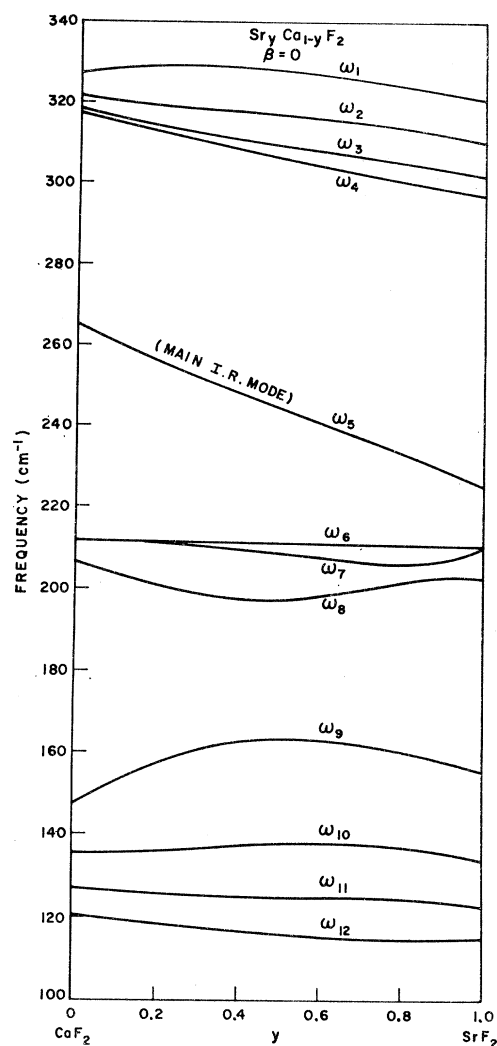


FIG. 9. Infrared-active mode frequencies for  $\text{Sr}_y\text{Ca}_{1-y}\text{F}_2$  versus composition ( $y$ ) computed from the model for  $\beta=0$ .

values of  $\beta$  cannot be used over the entire range of  $y$  as explained previously. The use of  $\beta=-0.15$  for the  $y=0.5$  barium-strontium-fluoride crystal is discussed below.

The most significant feature of Figs. 10 and 11 is that one mode in each system (the main I.R. mode) predominates in strength over the other modes. This result also holds for other values of  $\beta$ . The eigenvector of this mode shows it to be due to vibrations of all F ions against all the cations. This is very different from what we found in  $\text{GaAs}_y\text{P}_{1-y}$  and in  $\text{CdSe}_y\text{S}_{1-y}$ . There

the two main modes were due predominantly to vibrations of cations against anions in units 1 for the lower frequency mode and cations against anions in unit 5 for the higher-frequency mode. We will return to this point later since it allows us to make contact with the virtual-ion model.

The group of four high-frequency modes ( $\omega_1$  to  $\omega_4$ ) and the group of three modes with frequencies somewhat lower than the main mode ( $\omega_6$  to  $\omega_8$ ) are similar in nature to the modes found to exist in  $\text{GaAs}_y\text{P}_{1-y}$  and  $\text{CdSe}_y\text{S}_{1-y}$ . The eigenvectors of these modes show them to be predominantly due to vibrations within a particular unit. The nature of these modes changes, how-

modes, presumably because of the relatively large  $F_1$ - $F_2$  force constants are no longer negligible in these mixed fluorides, especially in  $\text{Sr}_y\text{Ca}_{1-y}\text{F}_2$ .

The frequencies of the Raman modes as a function of  $y$  are plotted in Figs. 12 and 13, together with the strengths of the main modes. The linear dependence of the frequency of the main Raman modes in  $\text{Sr}_y\text{Ca}_{1-y}\text{F}_2$  is in agreement with the experimental results of Chang *et al.*<sup>1</sup> The combined strength of the other four modes given by the model is less than  $\frac{1}{2}\%$  of the strength of the main mode. They were not observed by Chang *et al.*<sup>1</sup>

In  $\text{Ba}_y\text{Sr}_{1-y}\text{F}_2$  the total Raman strength is divided between the two highest-frequency modes as is shown in Fig. 12. The three lower-frequency modes have negligible strength as in  $\text{Sr}_y\text{Ca}_{1-y}\text{F}_2$ . Chang *et al.* report only a single Raman mode. However, the linewidth of this mode was about  $10\text{ cm}^{-1}$ . Between  $y=0.5$  and  $y=0.8$ , where according to our model the two modes both have

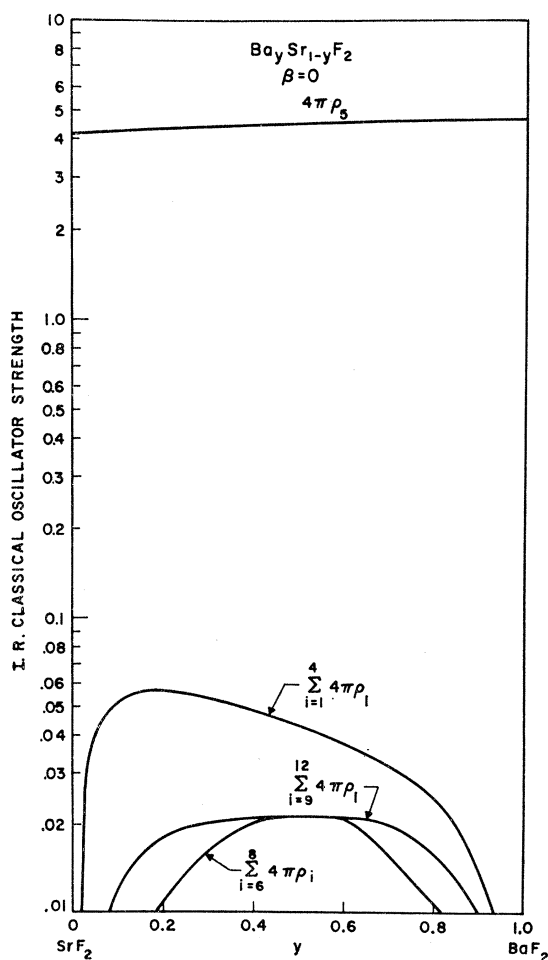


FIG. 10. Infrared-active model strengths for four groups of modes in  $\text{Ba}_y\text{Sr}_{1-y}\text{F}_2$  versus composition ( $y$ ) computed from the model for  $\beta=0$ .

ever, with composition. For example, mode 6 in  $\text{Ba}_y\text{Sr}_{1-y}\text{F}_2$  is mainly due to F-Ba vibrations in unit 1 for small values of  $y$ , but changes its character to  $F$  vibrating against Ba and Sr in unit 2 at large values of  $y$ .

The group of four low-frequency modes are very similar to those found in  $\text{GaAs}_y\text{P}_{1-y}$  and consist of relative vibrations of entire units. The strengths of these

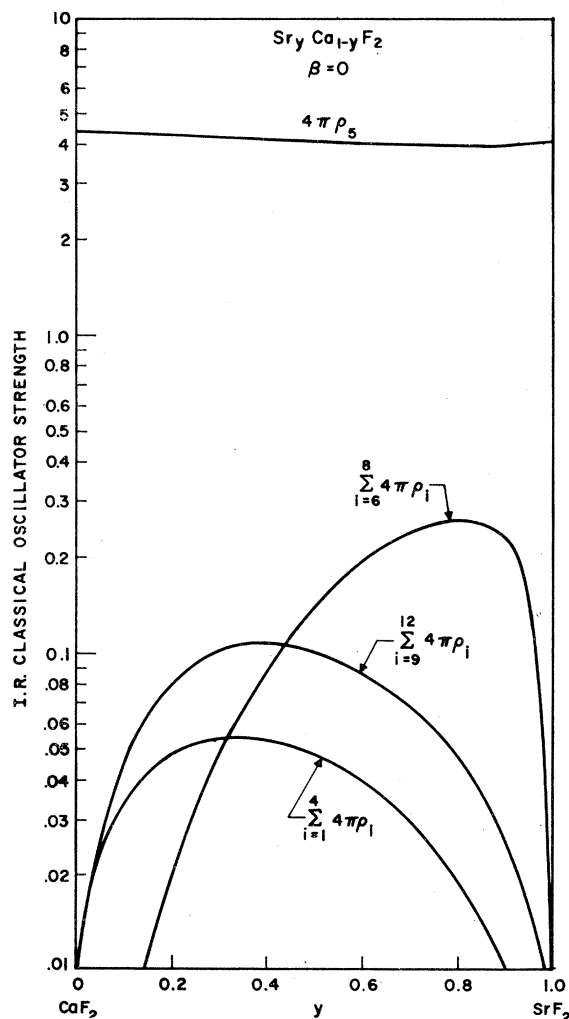


FIG. 11. Infrared-active mode strengths for four groups of modes in  $\text{Sr}_y\text{Ca}_{1-y}\text{F}_2$  versus composition ( $y$ ) computed from the model for  $\beta=0$ .

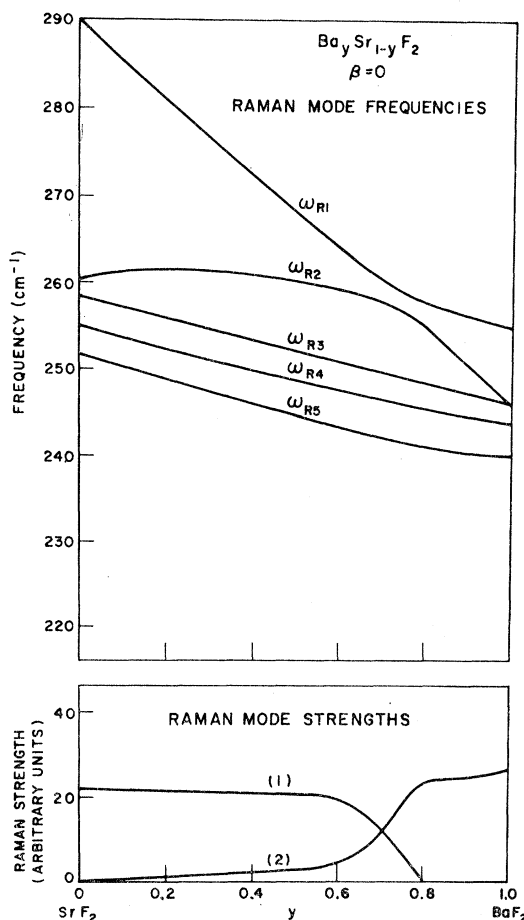


FIG. 12. Raman-active model frequencies and strengths for  $\text{Ba}_y\text{Sr}_{1-y}\text{F}_2$  versus composition ( $y$ ) computed from the model for  $\beta=0$ . Only the strengths of modes (1) and (2) are shown. The other modes have negligible strengths.

considerable strength, their frequencies are less than  $10\text{ cm}^{-1}$  apart and might, therefore, not be experimentally resolved.

In Figs. 14, 15, and 16 we present the theoretical fits to the reflectivity spectra at  $90^\circ\text{K}$  for three mixed crystals of  $\text{Ba}_y\text{Sr}_{1-y}\text{F}_2$ . The mode parameters: frequency  $\omega$ ; strength  $4\pi\rho$ , and linewidth  $\Gamma$ , as well as  $\beta$  and  $\epsilon_\infty$  are listed in each figure. With the exception of the highest-frequency mode which we interpret as a combination band, the values for the strength and frequency of each mode are those given by the model. The linewidth of each mode is chosen to give a best fit and is found to have values typical of the linewidth of phonons in pure crystals.

As mentioned earlier, we find both experimentally and theoretically that the spectrum at each value of  $y$  is predominantly due to a single strong resonance mode. The weak lowest frequency band predicted by the model has little effect on the reflectivity spectrum. The experimental results are consistent with the presence of such a band but its presence is not positively confirmed. The readily observable fine structure on top of the

reststrahlen bands is caused by a band of three weak modes given by the model. We take this structure to be a significant mixed-crystal effect as opposed to combination band effects which of course must also be present. As has been discussed previously, the appearance of such structure as well as the actual concentration dependence of the main mode frequency and strength rule out the use of the virtual-ion model for a detailed description of these mixed crystals.

A best fit at  $y=0.5$  required a negative value for  $\beta$ . At the other compositions, choosing a nonzero  $\beta$  did not improve the fit. We, therefore, took  $\beta=0$  at all other concentrations. The negative value for  $\beta$  at  $y=0.5$  suppresses the strength of the mode at  $283\text{ cm}^{-1}$  and increases the main mode strength, greatly improving the fit. The eigenvector of the  $283\text{ cm}^{-1}$  mode shows that its strength is predominantly due to vibrations of Sr ions against F ions in unit 5 (see Fig. 6). When  $\beta=-0.15$  the number of these units in the lattice is considerably reduced and the number of type-3 units is increased. This tendency towards type-3 units is an ordering tendency. A case of extreme ordering in  $\text{Ba}_{0.5}\text{Sr}_{0.5}\text{F}_2$  is achieved by making (100) cation planes

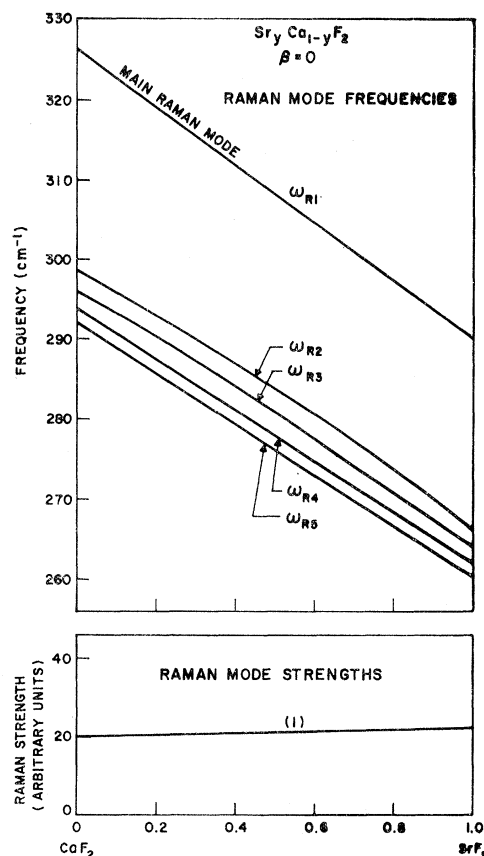


FIG. 13. Raman-active model frequencies and strengths for  $\text{Sr}_y\text{Ca}_{1-y}\text{F}_2$  versus composition ( $y$ ) computed from the model for  $\beta=0$ . Only the strength of mode (1) is shown. The other modes have negligible strengths.

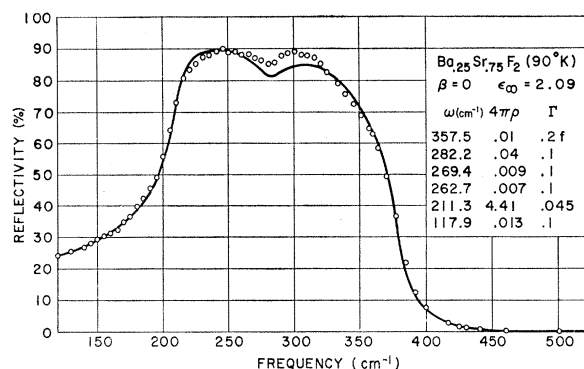


FIG. 14. Theoretical fit (solid line) to experimental reflectivity data for  $\text{Ba}_{0.25}\text{Sr}_{0.75}\text{F}_2$ . The oscillator parameters and  $\beta$  value are listed in the figure. The mode labeled *f* is the combination band described in the text.

alternately all Sr ions then all Ba ions. The crystal then consists entirely of type-3 units.

There are some weak second-order or combination bands present in both  $\text{BaF}_2$  and  $\text{SrF}_2$ . Evidence for the existence of a weak mode in the mixed crystals whose frequency varies linearly between the frequency of the weak mode in  $\text{BaF}_2$  ( $320\text{ cm}^{-1}$ ) and that in  $\text{SrF}_2$  ( $370\text{ cm}^{-1}$ ) is presented in Fig. 16. This is the highest-frequency mode mentioned earlier which is not given by the model. The dotted line there represents a fit with a

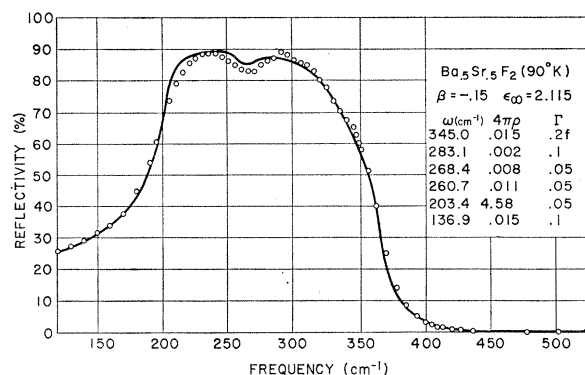


FIG. 15. Theoretical fit (solid line) to experimental reflectivity data for  $\text{Ba}_{0.5}\text{Sr}_{0.5}\text{F}_2$ . The oscillator parameters and  $\beta$  value are listed in the figure.

mode at  $335\text{ cm}^{-1}$  left out. The solid line is the theoretical fit with this mode included and is decidedly better. We take this mode to be a combination band or at least not a specific mixed-crystal effect and label it *f* in the figure.

The theoretical fits to the reflectivity spectra of  $\text{Sr}_y\text{Ca}_{1-y}\text{F}_2$  at  $90^\circ\text{K}$  are presented for three values of  $y$  in Figs. 17, 18, and 19. The mode parameters are again listed in each figure. We find that in all cases  $\beta=0$  gives the best fits. The results here are not as good as in the previous system. We note especially the poor fit to the experimental data at the low-frequency side of the reststrahlen bands. We did attempt to obtain a better

fit in that region for the  $y=0.515$  crystal by introducing additional *ad hoc* modes near  $260\text{ cm}^{-1}$ , but were not successful. A Kramers-Kronig analysis of the experimental reflectivity shows that the shape of the reflectivity is not due to resolvable modes but to a rather nonsymmetric mode shape which is most naturally described by a frequency-dependent damping parameter. It was felt that the introduction of additional parameters to describe frequency-dependent damping would not be particularly illuminating, and this was not attempted. The behavior here does suggest the possibility of increased coupling of the main optic mode to the two-phonon density of states because of disorder in

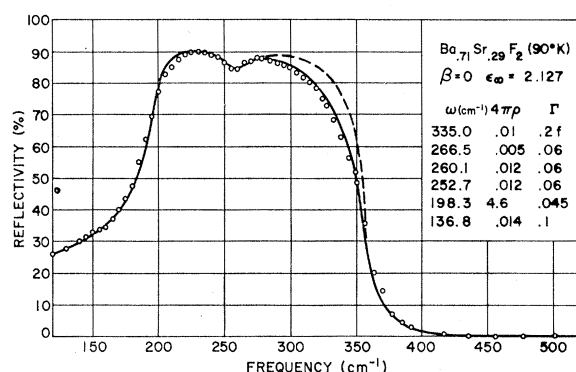


FIG. 16. Theoretical fit (solid line) to experimental reflectivity data for  $\text{Ba}_{0.71}\text{Sr}_{0.29}\text{F}_2$ . The oscillator parameters and  $\beta$  value are listed in the figure.

the mixed crystals. Such increased coupling is also suggested by the increase of the damping parameter of the main mode as  $y$  approaches 0.5.

The second-order or combination modes observed in  $\text{CaF}_2$  and  $\text{SrF}_2$  also extend into the mixed-crystal system. We have indicated these modes on the lists of mode parameters (symbol *f*) in each figure. The effect of these modes is similar to what was observed in  $\text{Ba}_y\text{Sr}_{1-y}\text{F}_2$ . We note again that the strength and frequencies of these modes are not given by the model, but were merely chosen to give a better fit.

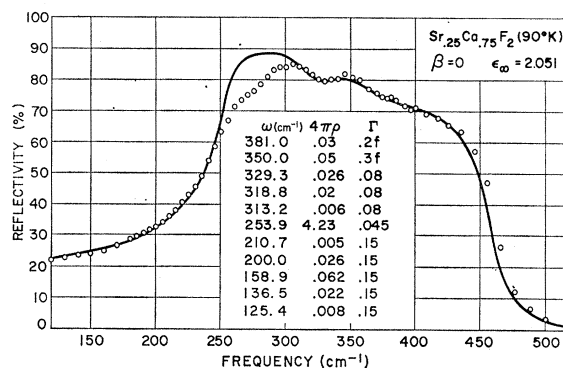


FIG. 17. Theoretical fit (solid line) to experimental reflectivity data for  $\text{Sr}_{0.25}\text{Ca}_{0.75}\text{F}_2$ . The oscillator parameters and  $\beta$  value are listed in the figure.

TABLE V. Displacements of ions in strongest infrared and Raman modes of  $\text{Ba}_{0.5}\text{Sr}_{0.5}\text{F}_2$ . Force constants and charges are given in Table IV. For comparison the two main modes in  $\text{CdSe}_{0.53}\text{S}_{0.47}$  are also given.

Unit <i>i</i>	<i>f<sub>i</sub></i> % present	Ion type	Ba <sub>0.5</sub> Sr <sub>0.5</sub> F <sub>2</sub>		CdSe <sub>0.53</sub> S <sub>0.47</sub>		Ion type	<i>f<sub>i</sub></i> % present
			Displacements IR mode 202 cm <sup>-1</sup>	(β = -0.15)	Displacements IR mode 1 177 cm <sup>-1</sup>	(β = 0.40)		
				Raman mode 267 cm <sup>-1</sup>		IR mode 2 251 cm <sup>-1</sup>		
1	1.5	F1	0.45	0.28				
		F2	0.45	-0.28				
		Ba	-0.099	0.0	-0.29	0.01	Cd	24
2	24	F1	0.40	0.31	0.43	-0.05	Se	
		F2	0.40	-0.31	-0.04	-0.02	Cd	23
		Ba	-0.104	0.0	0.08	-0.04	Se	
3	49	Sr	-0.118	0.0	0.01	0.41	S	
		F1	0.34	0.37				
		F2	0.34	-0.37	-0.01	-0.05	Cd	14
4	24	Ba	-0.103	0.0	0.02	-0.03	Se	
		Sr	-0.135	0.0	0.04	0.38	S	
		F1	0.28	0.469	-0.01	-0.14	Cd	19
5	1.5	F2	0.28	-0.469	-0.04	0.04	Se	
		Ba	-0.096	0.0	-0.04	0.04	Se	
		Sr	-0.143	0.0	0.06	0.76	S	
		F1	0.20	1.28				
		F2	0.20	-1.28	-0.02	-0.12	Cd	20
		Sr	-0.137	0.0	0.05	0.53	S	
			V.I. Model					
			F1	0.34	0.34			
			F2	0.34	-0.34			
			(BaSr)	-0.115	0.0			

The model does predict modes near 310  $\text{cm}^{-1}$  which as in  $\text{Ba}_y\text{Sr}_{1-y}\text{F}_2$  produce the fine structure on top of the reststrahlen bands. The modes with frequencies lower than the main I.R. mode have considerably more strength than those in  $\text{Ba}_y\text{Sr}_{1-y}\text{F}_2$ , however their effect on the reflectivity spectra is merely to increase the reflectivity at the low-frequency side of the reststrahlen bands.

The main feature of the infrared spectra of both systems is thus the predominance of a single, strong mode with some weak additional modes causing the fine structure of the reststrahlen bands. From the model we find that there is also one main Raman mode. Its frequency varies linearly with composition. A comparison has already been published<sup>3</sup> of the fit of the calculated Raman mode with the data of Chang *et al.*<sup>1</sup> In Table V we list the ion displacements of the main in-

frared and Raman modes in  $\text{Ba}_{0.5}\text{Sr}_{0.5}\text{F}_2$ . We note that within any unit the qualitative form of the displacements is the same as for the pure crystal (Table II); however, for the I.R. mode the ratio of anion-to-cation displacement is no longer given by a simple mass factor.

#### Comparison of the Model with a Virtual-Ion Model

In Ref. 3 we have given a preliminary comparison of the virtual-ion (V.I.) model with the detailed model presented in the present paper. The basic approximations which lead to the virtual-ion concept for problems of band structure or lattice vibrations have been discussed by Herman *et al.*<sup>16</sup> For the infrared-active mode of vibration, the virtual-ion approximation consists of defining a virtual cation with average properties. This virtual ion is then imagined to reside at every cation site in the lattice restoring the translational symmetry. In  $\text{Ba}_y\text{Sr}_{1-y}\text{F}_2$  the virtual cation would have mass

$$ym_{\text{Ba}} + (1-y)m_{\text{Sr}}.$$

One takes a similar composition-dependent average of the cation-anion force constants, the charges, the lattice constants and the high-frequency dielectric constants. Following the procedure previously outlined for the pure crystals, we then calculate the infrared frequencies and strengths.

For the Raman mode, Table II shows that the cation mass does not enter the frequency expression. The virtual cations do control  $k_1$  and  $k_6$  however, so concentration-weighted averages of these forces are formed.

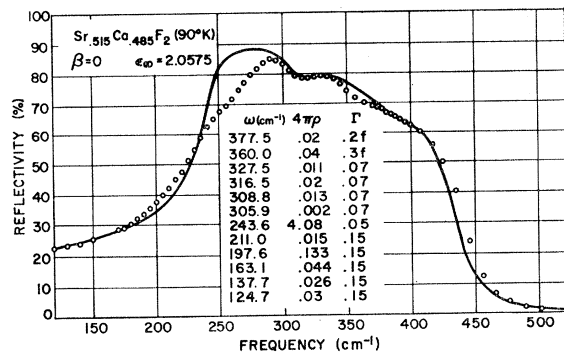


FIG. 18. Theoretical fit (solid line) to experimental reflectivity data for  $\text{Sr}_{0.515}\text{Ca}_{0.485}\text{F}_2$ . The oscillator parameters and  $\beta$  value are listed in the figure.

<sup>16</sup> F. Herman, M. Glicksman, and R. H. Parmenter, *Progress in Semiconductors* (John Wiley & Sons, Inc., New York, 1957), Vol. 2.

Since  $\omega_R^2 = (k_1 + k_6)/m_F$  we note that  $\omega_R^2$  will vary linearly with composition for the virtual-ion (V.I.) model. For the actual force constants and the mass used in these fluoride mixed crystals we find that  $\omega_R$  itself varies almost linearly with composition. The deviation from linearity of the frequency is only about  $\frac{1}{4}\%$  high for the virtual-ion model at  $y=0.5$ . Figure 20 shows the V.I. model calculations as dashed curves. The Raman frequencies given by the V.I. model coincide with the frequencies of mode 1 in our model at low values of  $y$ , and with the frequencies of mode 2 at large values of  $y$ . Both results agree with experiment since the two modes given by our model cannot be resolved experimentally in the region between  $y=0.6$  and  $0.8$  where the two modes have comparable strengths.

The two models disagree in their predictions of the infrared frequencies and strengths. Our results are in closer agreement with experiment than those given by the V.I. model. The strength of the main I.R. mode at  $y=0.5$  is somewhat higher than the calculated value for  $\beta=0$ . Taking  $\beta=-0.15$ , as was done in the fit presented in Fig. 15, brings the calculated and experimental values of the strength of the main mode in agreement, giving a good fit for all concentrations. In addition to disagreement concerning the infrared mode strength and frequency, the V.I. model does not account for the fine structure which is experimentally observed. In Fig. 21 we present a fit to the reflectivity spectrum of  $\text{Ba}_{0.5}\text{Sr}_{0.5}\text{F}_2$  using the V.I. model results to illustrate this last point. This figure is to be compared with the fit based on our model presented in Fig. 15, which, as can be seen, is considerably better.

An interesting comparison can be made between the eigenvectors of our model and the V.I. model. Table V shows that at  $y=0.5$  unit 3 is the most prevalent ion complex. The strongest I.R. mode consists of F ions moving 0.34 units along  $z$  (Fig. 5) in unit 3, Sr ions moving  $-0.135$  units, and Ba ions moving  $-0.103$  units. The V.I. model has a slightly higher frequency for this mode and would have both F ions moving 0.34 units and one virtual (Ba-Sr) ion moving  $-0.115$  units

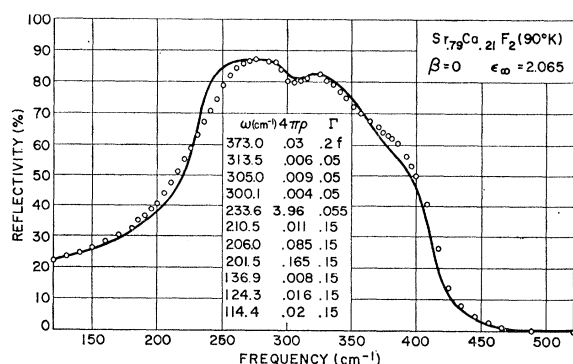


FIG. 19. Theoretical fit (solid line) to experimental reflectivity data for  $\text{Sr}_{0.79}\text{Ca}_{0.21}\text{F}_2$ . The oscillator parameters and  $\beta$  value are listed in the figure.

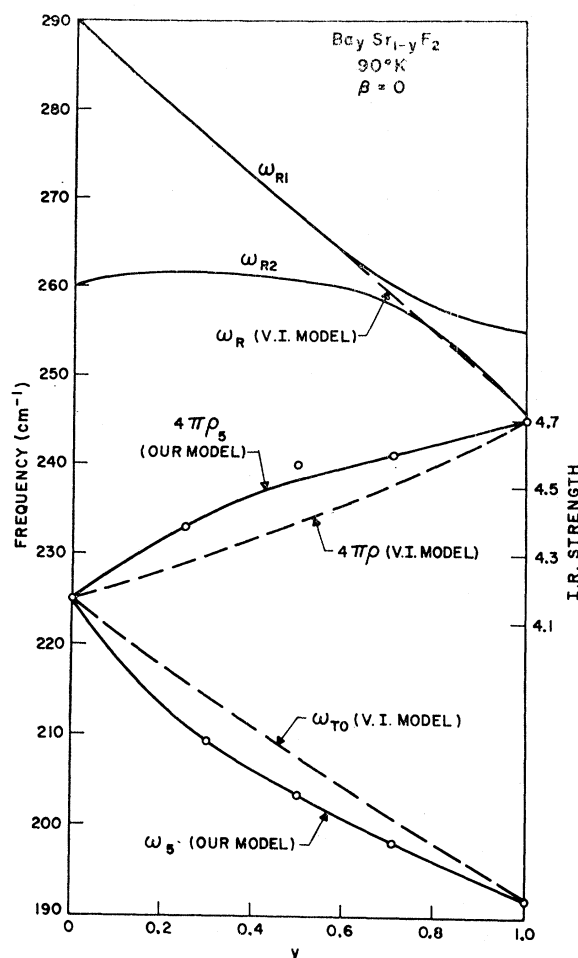


FIG. 20. Comparison of infrared and Raman frequencies as well as infrared oscillator strength ( $4\pi\rho$ ) for  $\text{Ba}_y\text{Sr}_{1-y}\text{F}_2$  as calculated from our model and from a virtual-ion model.

along  $z$  in each primitive cell. Our model has in addition, Ba and Sr ions moving with slightly different amplitudes in other less prevalent units. We find therefore that in our model the motion is predominantly like the

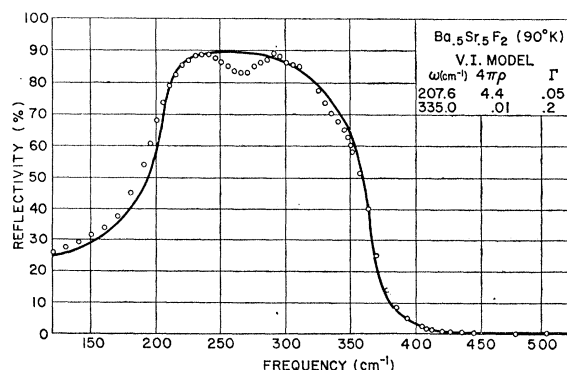


FIG. 21. Theoretical fit (solid line) based on V.I. model to experimental reflectivity data for  $\text{Ba}_{0.5}\text{Sr}_{0.5}\text{F}_2$ . The mode at  $207.6\text{ cm}^{-1}$  is predicted by the V.I. model. The second weak mode at  $335\text{ cm}^{-1}$  is the same combination band used in Fig. 15.

virtual-ion model motion but there is a small relative motion of Ba and Sr; moreover, Ba and Sr ions in different environments (units) move with slightly different amplitudes. These slight relative cation motions bring into play second-neighbor forces and electrostatic forces which change the frequency from the V.I. model prediction. In addition, allowing relative motion for cations in different environments yields the other weaker modes (not shown in Table V) which fit the structure shown in Fig. 15.

We also show in Table V the ion displacements in a mixed crystal whose force constants, masses, and charges cause two widely separated modes in the  $y=0$  and  $y=1$  pure crystals. There is very little tendency here towards virtual-ion behavior. The behavior of this crystal system has been discussed previously.<sup>8</sup> We note here that near  $y=0.5$  there is not one main infrared mode but two. The lower-frequency eigenvector consists of the heavier anion moving against the cation (mostly in unit 1) while the higher-frequency mode consists predominantly of the lighter anion moving against the cation in units 3 and 4. This distinct two-mode behavior cannot be approximated by a simple virtual-ion model.<sup>3</sup>

## V. CONCLUSIONS

We have shown in this paper that a conceptually simple model of a mixed crystal which was originally developed to explain the reflectivity spectra of  $\text{GaAs}_y\text{P}_{1-y}$  and  $\text{CdSe}_y\text{S}_{1-y}$ , i.e., systems having two reststrahlen bands, is applicable also to these mixed fluorides which have only a single reststrahlen band. This seems to lead to the conclusion, therefore, that there is no fundamental difference between these two kinds of systems. In particular it seems unnecessary to associate single-band systems with homogeneous mixtures and the two-band systems with imperfect solid solutions. In the application of the model to the two-band systems ( $\text{GaAs}_y\text{P}_{1-y}$  and  $\text{CdSe}_y\text{S}_{1-y}$ ),  $\beta$  had rather large positive values suggesting a strong degree of clustering of like anions around the cations, whereas in these mixed fluorides  $\beta$  is found to be zero (i.e., like ions are not clustered) and in one case negative for good fits to the reflectivity spectrum. As was shown in I and II,  $\beta$  does not control the appearance of one or two bands; thus the nonclustered arrangement of the ions

is not directly related to the appearance of one main mode in these crystals. Chang *et al.*<sup>1</sup> have speculated that the ions are distributed randomly ( $\beta=0$ ). However, independent measurement would be valuable to establish this point. This may be possible using small-angle x-ray scattering.

The appearance of one or two bands in the reflectivity and Raman spectra of mixed crystals depends primarily on the relative values of the atomic masses and force constants of the two parent crystals, or equivalently on the separation and relative strengths of the Raman and infrared modes in these crystals.<sup>3</sup>

One of the predictions of the model is the appearance of weakly infrared-active modes at frequencies below the main TO band. In an attempt to verify the existence of these weak modes we have made transmission measurements on a mixed crystal of strontium-calcium fluoride in the range 180 to 250  $\text{cm}^{-1}$ . Unfortunately the transmission is so low for the thinnest samples which could be prepared that a weak band near 210  $\text{cm}^{-1}$  could not be ruled out or confirmed. A separate neutron diffraction study of  $\text{Ba}_{0.5}\text{Sr}_{0.5}\text{F}_2$  is being planned which should give valuable independent evidence of the optic mode structure.

Finally, we have seen that the V.I. model, while applicable to the Raman spectrum of the mixed fluorides, falls short when applied to the infrared reflectivity spectrum of the mixed fluoride systems. Its complete failure in explaining the two reststrahlen band systems was already noted.<sup>3</sup> The basic difference between this and our model lies essentially in the fact that the V.I. model averages the lattice vibration properties of the pure materials, assuming both cations will vibrate as they did in the pure crystal. This approach is obviously violated in the case where a light component forms a local mode and vibrates independently. Our model retains the individual character of the two components and assumes that the cation-anion interaction of one component is perturbed by the presence of the other material in the lattice. Only when the pertinent properties of the two parent crystals are very close do the two models yield similar results.

## ACKNOWLEDGMENT

The authors wish to express their gratitude to Dr. D. E. McCumber for helpful discussions.